Paper No. 140. (quote when citing this article)
Eleventh World Conference on Earthquake Engineering
ISBN: 0 08 042822 3

SIMULATION OF THE BOREHOLE RECORDS OBSERVED AT THE PORT ISLAND IN KOBE, JAPAN, DURING THE HYOGO-KEN NANBU EARTHQUAKE OF 1995

H. KAWASE, T. SATOH, and K. FUKUTAKE

Izumi Research Institute, Shimizu Corp., Fukoku Seimei Bldg, 2-2-2, Uchisaiwai-cho, Chiyoda-ku, Tokyo, 100 Japan

ABSTRACT

Strong motion records of the Hyogo-ken Nanbu earthquake of 1995 observed by the borehole array at Port Island, Kobe, are analyzed to see the effects of soil nonlinearity. The horizontal peak accelerations and the predominant period on the surface are smaller and longer than those in the boreholes. We try to simulate the observed records by using 1-D equivalent linear and effective stress analyses with the reasonable soil constants derived from the boring survey. The equivalent linear analysis overestimates the surface records, while the effective stress analysis considering the excess pore water pressure (=liquefaction) reproduces the observed records on the whole. The estimated excess pore water pressure ratio in the reclaimed sand layers reaches to almost 1.0 within a few seconds from the start of strong shaking and they suffer maximum shear strain of more than 4%. The strong liquefaction in these shallow sand layers should act to reduce the structural damage in the areas close to shorelines and in the reclaimed land.

KEYWORDS

site effects; soil nonlinearity; equivalent linear analysis; effective stress analysis; liquefaction; reclaimed land; borehole observation; Port Island; strong motion; Kobe; the 1995 Hyogo-ken Nanbu earthquake

INTRODUCTION

The Hyogo-ken Nanbu earthquake of 1995 caused devastating damage to Kobe and surrounding areas. To understand the cause of the damage first we need to quantify the strength of input motions to structures in the area during the earthquake. In spite of aftermath difficulties several institutions collected observed strong motion data in the damage areas, one of which is the borehole records at Port Island, a big reclaimed land in Kobe Port. They are collected by the Kobe municipal government for investigation. These strong motion records are invaluable both from a geotechnical engineering aspect for nonlinear soil response studies and a structural engineering aspect for input motion evaluation. The surface records at Port Island clearly show nonlinear effects of soil response, namely, prolongation of the predominant period and lower amplitude in acceleration. It is evident that this nonlinearity came from the liquefaction of surface soils judging from sand boiling and subsequent land settlement caused by the earthquake throughout Port Island.

It is our urgent need to prove if the observed nonlinearity is really caused by the liquefaction and, if yes, then to show how strong it should be. In this paper we try to understand the phenomena associated with the soil nonlinearity through simulation analyses of the observed records at Port Island. First we inspect the observed records at Port Island and summarize their characteristics. Then we simulate them by using most plausible soil models and one-dimensional equivalent linear and true nonlinear analyses. The results presented here are still preliminary in the sense that we do not have collected yet detailed information on important nonlinearity parameters, nonetheless they undoubtedly suggest that the effects of liquefaction should be referred to whenever we consider the structural or lifeline damage in Kobe.

OBSERVED DATA AT PORT ISLAND

Strong motion observation at Port Island has started from November of 1991 by the development department of the Kobe municipal government. Fig.1 shows the location of the observation site. With the installation of stations they conducted geological survey and a P-S logging to obtain soil classification, SPT N-values, and P- and S-wave velocity profiles. Table 1 summarizes the information above the deepest borehole sensor 83m below the ground level, denoted here as GL-83m. The other two borehole sensors are at 16m and 32m below (GL-16m and GL-32m) and another sensor is on the surface (GL0m). Fig.2 shows first 20 seconds of the observed accelerograms (Note: initial 9 seconds is removed) of two horizontal components rotated to the major axis (N35°W) and to the minor axis (E35°N), and the vertical component. At GL-83m we need to rotate additional 20° clockwisely to obtain best long-period similarity to other data. No other stations need such a significant correction in their installed direction. We should note that very sharp peaks appear in the UD-component at GL-16m may not reflect the real ground motion there since these pulses do not propagate neither upward nor downward. We are speculating that these pulses are generated locally by some kind of debris colliding to the sensor floating in the boiling sand. Anyway it is apparent that in horizontal components shallower the station less amplitude in high frequency. In terms of peak ground acceleration (PGA), 720 Gals at GL-83m decreases to 425 Gals at GL0m. On the contrary, the vertical components show systematic amplification from the bottom to the surface (except for conspicuous peaks at GL-16m, of course). Relative amplification from GL-83m to GL0m is approximately 3.0 in the vertical component, and so PGA in the vertical component is 30% larger than those in the horizontal components on the surface. If we examine the horizontal components at GL0m closely we notice that period of each pulse is prolonged as time goes by.

To further demonstrate nonlinearity during the main shock we calculate Fourier spectral ratios between two stations at different depths for both the main shock and several aftershocks to find any difference. We obtained 6 aftershocks from January 26 to February 18 of 1995 whose PGAs are less than 35 Gals at GL-83m or 65 Gals at GL0m. Fig.3 shows spectral ratios GL0m/GL-32m and GL-32m/GL-83m for horizontal components. Thick solid and dotted lines are for the main shock (major- and minor-axis) and thin lines are for aftershocks. It is clear that predominant peaks apparent in the aftershock spectral ratios disappear completely from the main shock ratios not only for the spectral ratios GL0m/GL-32m but also for those GL-32m/GL-83m. Very small values of amplification in the high frequency range of the ratios GL0m/GL-32m during the main shock reflect strong nonlinear behavior of soil to filter out high frequency component. On the other hand the ratios GL-32m/GL-83m during the main shock fluctuate around unity very gently, which means that these two borehole records are essentially identical and that there exist very little reflecting waves in these records.

EQUIVALENT LINEAR ANALYSIS

Based on the soil properties shown in Table 1, we simulate the observed main shock motions using one-dimensional equivalent linear analyses. The observed records at GL-83m are used as input motions. We assume a frequency dependent damping as $h_0 f^{-0.7}$ based on the previous study in Sendai, Japan (Satoh *et al.*, 1995a). Nonlinearity parameters such as shear modulus reduction curves and damping curves are assumed as a function of soil types and the effective overburden pressure (AIJ, 1993). A numerical method to calculate transfer functions is a modified version (Satoh *et al.*, 1995b) of the so-called SHAKE (Schnabel *et al.*, 1972). Fig.4 shows (a) acceleration and (b) velocity time histories obtained by the equivalent linear simulation. These are for N32°W component (Note: 3° difference from Fig.2 is due to the definition of principal axes) using the record shown at the bottom, which is band-pass filtered between 0.1Hz and 5 Hz. It is clear that the equivalent linear method does very good job up until GL-16m but it fails to reproduce the records on the surface. The difference in the first 5 seconds is relatively small but then it becomes larger and larger. It suggests that the liquefaction may have happened at around 5 seconds. Compared to the linear simulation that gives more than 1,200 Gals on the surface, the equivalent linear simulation does much better job, although it still overestimates PGA by 50%.

Fig.5 shows distributions of the effective shear strain, the shear modulus reduction factor, and the damping coefficient at 1 Hz ($=h_0$) in the equivalent linear simulation. We found that the sand and gravel layers between GL-9m to GL-19m suffered strongest shear strain reaching to the order of 1% . As a result of such high strain the shear modulus reduction factors and the damping coefficients reach to less than 0.1 and more than 0.20, respectively. As for the minor-axis input the level of nonlinearity is much less than the major-axis input.

EFFECTIVE STRESS ANALYSIS

From the equivalent linear analysis it turns out that we need to use more sophisticated method to reproduce the observed records on the surface. Since other pieces of information unanimously show that soils in Port Island

are liquefied by very intense shaking there, we try to simulate the records by using a one-dimensional nonlinear soil model taking into account effects of excess pore water pressure. Unfortunately necessary model parameters for this type of analyses that control behavior of soil toward liquefaction are vastly unknown at the time of analysis so that we have to assume most plausible values from available information such as soil types, SPT N-values, age, and P- and S-wave velocities.

The effective stress analysis code used here is called "ALISS" and is a two-dimensional nonlinear finite element code in time-domain developed by Ohtsuki and Fukutake (Ohtsuki and Ito, 1987; Fukutake *et al.*, 1990). The constitutive relationship between shear strain and stress in the code is the well-established Ramberg-Osgood model that expresses nonlinear behavior of soil in the laboratory test very well. The effects of excess pore water pressure including cyclic mobility are expressed by the so-called "Bowl model" proposed by Fukutake and Matsuoka (1989). The analysis is carried out under undrained condition since duration of strong motion is very short, about 10 seconds.

As stated above we assume model parameters that control nonlinear behavior of soil, such as shear strain level of normalization ($\gamma_{0.5}=\gamma$ at which $G/G_0=0.5$), maximum damping factor h_{max}, and liquefaction strength, for each layer of soil based on our previous simulations and information at Port Island shown in Table 1. The only modification we made is the S-wave velocity of the No.4 layer in Table 1; we increased it from 210 m/sec to 240 m/sec based on the SPT N-values of the layer. It contributes to prevent too strong concentration of strain in this layer to some extent. The water level is assumed to be GL-4m that corresponds to the average sea level at Kobe Port. We applied the observed accelerogram at GL-83m to the bottom of a one-dimensional finite element column as an input. The target frequency range is 0.1 Hz to 5.0 Hz so that we divide each layer into small sells to represent waves in that frequency range. We applied a band-pass filter of that range to the input motion. Both the major-axis (N32°W) and minor-axis (E32°N) input motions are used independently. In fact we have already done a coupling analysis applying two components at the same time and found that the major-axis input yields almost identical results with the coupled input while the minor-axis input does not.

First let us show you results for the major-axis input. Fig.6 compares simulated acceleration and velocity time histories with the observed ones. The bottom traces are again input motions at GL-83m. From this figure we can say that we succeed to reproduce waveforms of the surface record remarkably well for both in acceleration and velocity. Although there exist small discrepancies from time to time, overall fitness is fairly good, especially in the later part. PGA of the simulation is only 10% and PGV is 20% higher than the observed.

In Fig.7 we plot acceleration time histories for the minor-axis input in the same manner as in Fig.6(a). The simulation apparently overestimates the observed surface motion. This means that nonlinearity of soils in the minor-axis is primarily not controlled by the input in that direction but by the excess water pressure built up by the strong shaking in the major-axis. As stated above we have already confirmed it by a coupling analysis.

In Fig.8 we show time histories of the excess pore water pressure ratios calculated in the finite elements at several depths for both major- and minor axis inputs. The excess pore water pressure ratio is the excess pore water pressure divided by the initial effective stress at that depth. If it reaches to 1.0, then it means that liquefaction happens since no confining stress for sand grains exists. In the simulation we restrict the value not to exceed 0.99 for numerical stability. The top trace corresponds to a layer above the water table so there is no pore water pressure. We obtain the limit value of 0.99 in the layer from GL-9.0m to -16.0m and high values in between GL-16.0m and -19.0m and also GL-29m and -32m. We should note that in these layers the excess pore water pressure build up very quickly and reach to the final level within a few seconds. This is a strong contrast to the previous case studies found in the literature where water pressure build-up process is relatively slow. The layer from GL-19m to GL-27m is a Holocene clay layer so that very small ratios are obtained. The timing of liquefaction for the shallow layers shown in this figure, at around 5 seconds, is in good agreement with the aforementioned timing from the equivalent linear analysis. For the minor-axis input shown by dotted lines the ratios are considerably smaller than those for the major-axis input.

Finally we show in Fig.9 the calculated distributions of the maximum shear strain, the excess pore water pressure ratio, and PGA along the vertical direction for both the major- and minor-axis inputs. As stated above the excess pore water pressure ratios reach to the values very close to 1.0 from GL-9.0m to -19m and the maximum shear strains in these layers become more than 4% for the major-axis input. As a result of this strong nonlinearity associated with the liquefaction PGA distribution shows gradual decrease from the peak at around GL-30m to GL-10m. From GL-10m to the surface slight increase of PGA is found probably due to the amplification by the layers above the water table. The deeper Holocene sand layers 27m to 37m below the surface also show high values of the excess pore water pressure ratios, however, their strain level remains in the order of 1%. In minor-axis input a PGA filtering effect is clearly be seen in the observation (solid circles) but not in the simulation since we do not consider here effects of the pore water pressure built up by the major-axis input.

CONCLUSIONS

By using the borehole records observed at Port Island during the 1995 Hyogo-ken Nanbu earthquake we have learned a lot on the nonlinear response of soil layers under very intense shaking. First we presented observed seismograms at all four level from the surface to 83m below and described their characteristics. Then we compare spectral ratios between up-hole/down-hole pairs for the main shock and aftershocks to find remarkable difference between them. To simulate the observed strong motion we conducted first an equivalent linear analysis to have good fittings up to GL-16m but not on the surface. Finally we performed a true nonlinear analysis in time domain considering the excess water pressure to have very good reproduction of observed records including that on the surface. The major conclusions are summarized as follows:

(1) Borehole accelerograms of horizontal components share more or less similar characteristics, however, the surface ones have distinctive characteristics from borehole ones, namely, much less high frequency component, 30% to 60% reduction in PGA, and much longer periods of motion.
(2) Spectral ratios between the surface and the borehole stations and between two borehole stations for the main shock and aftershocks show drastic reduction of amplification during the main shock in the upper 32m layers. Below 32m amplification between two borehole stations is almost equal to unity suggesting no reflection of wave at the surface is taking place.
(3) The simulated surface motion by an equivalent linear analysis has PGA 50% more than the observed and shows marked difference from about 5 seconds, suggesting that liquefaction started at around that time.
(4) A liquefaction analysis that considers the excess pore water pressure yields surface motions very similar to the observed. Its PGA is only 10% larger than and its PGV is 20% larger than the observed. The excess pore water pressure ratios in the sand and gravel or sand with gravel layers from GL-9.0m to -19m are estimated to be very close to 1.0 and their maximum shear strains to be more than 4%, which suggests complete liquefaction in these layers. In the minor-axis input its level is considerably less than that in the major-axis input so that the extent of liquefaction obtained is much less than the observed. Thus we need to consider directional coupling for quantitative simulation in both components at the same time.

Both the observed records and the simulated time histories show that the surface acceleration in the reclaimed land is strongly reduced by the liquefaction of shallow sand layers. Such filtering effects of liquefied sand has been suggested to emerge in the computer simulation well before the Hyogo-ken Nanbu earthquake but this earthquake provides its concrete evidence for the first time. This implies that small numbers of heavily damaged buildings and residential houses in the area close to shorelines as well as in the reclaimed land should be a direct consequence of liquefaction. Thus we must consider the effects of liquefaction whenever we estimate strong motions in Kobe for structural or lifeline studies. The results of the effective stress analysis presented here seem to be very encouraging since it reproduced the observed motions quite successfully using model parameters assumed only from available information.

ACKNOWLEDGMENTS

The authors wish to express their deep gratitude to the persons-in-charge of the Kobe municipal government and Prof. Kojiro Irikura of Kyoto University for providing us borehole records observed at Port Island.

REFERENCES

AIJ, Architectural Institute of Japan (1993). Subsurface investigation and soil dynamics, in *Earthquake Motion and Ground Conditions*, AIJ, Tokyo, Japan.

Fukutake, K. and H. Matsuoka (1989). A unified law for dilatancy under multi-directional simple shearing, *Proc. Japan Soc. Civil Eng.*, **412**/III-12, 240-248 (in Japanese).

Fukutake, K., A. Ohtsuki, M. Sato, and Y. Shamoto (1990). Analysis of saturated dense sand-structure system and comparison with results from shaking table test, *Earthquake Eng. Structural Dyn.*, **19**, 977-992.

Ohtsuki, A. and T. Ito (1987). Two-dimensional effective stress analysis of liquefaction of irregular ground including soil-structure interaction, *Earthquake Eng. Structural Dyn.*, **15**, 345-366.

Satoh, T., H. Kawase, and T. Sato (1995a). Evaluation of local site effects and their removal from borehole records observed in the Sendai region, Japan, *Bull. Seism. Soc. Am.*, **85**, No.6, 1770-1789.

Satoh, T., T. Sato, H. Kawase (1995b). Nonlinear behavior of soil sediments identified by using borehole records observed at the Ashigara Valley, Japan, *Bull. Seism. Soc. Am.*, **85**, No.6, 1821-1834.

Schnabel, P.B., J. Lysmer, and H.B. Seed (1972). A computer program for earthquake response analysis of horizontally layered sites, *Report EERC 72-12*, UCB, Berkeley, California, USA.

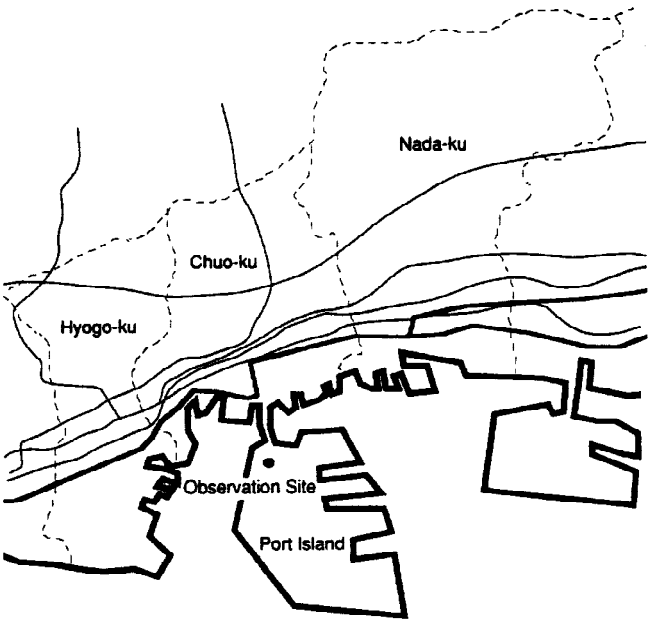

Fig.1 The location of the Port Island borehole site.

Table 1 Soil structure at the Port Island borehole site

No.	depth (m)	primary soil type		P-wave velocity (km/s)	S-wave velocity (km/s)	density (t/m^3)
1	0.0~2.0	sand and gravel	reclaimed soil	0.26	0.170	1.80
2	2.0~5.0	sand and gravel		0.33		1.80
3	5.0~12.6	sand and gravel		0.78	0.210	1.80
4	12.6~19.0	sand with gravel		1.48	0.240	1.80
5	19.0~27.0	clay	Holocene Ma13	1.18	0.180	1.50
6	27.0~37.0	sand	Holocene	1.33	0.245	1.85
7	37.0~50.0	sand with gravel	late Pleistocene	1.53	0.305	1.85
8	50.0~61.0	sand		1.61	0.350	1.85
9	61.0~83.0	clay	late Pleistocene Ma12		0.303	1.80
10	83.0~	sand with gravel	middle Pleistocene	2.00	0.320	1.90

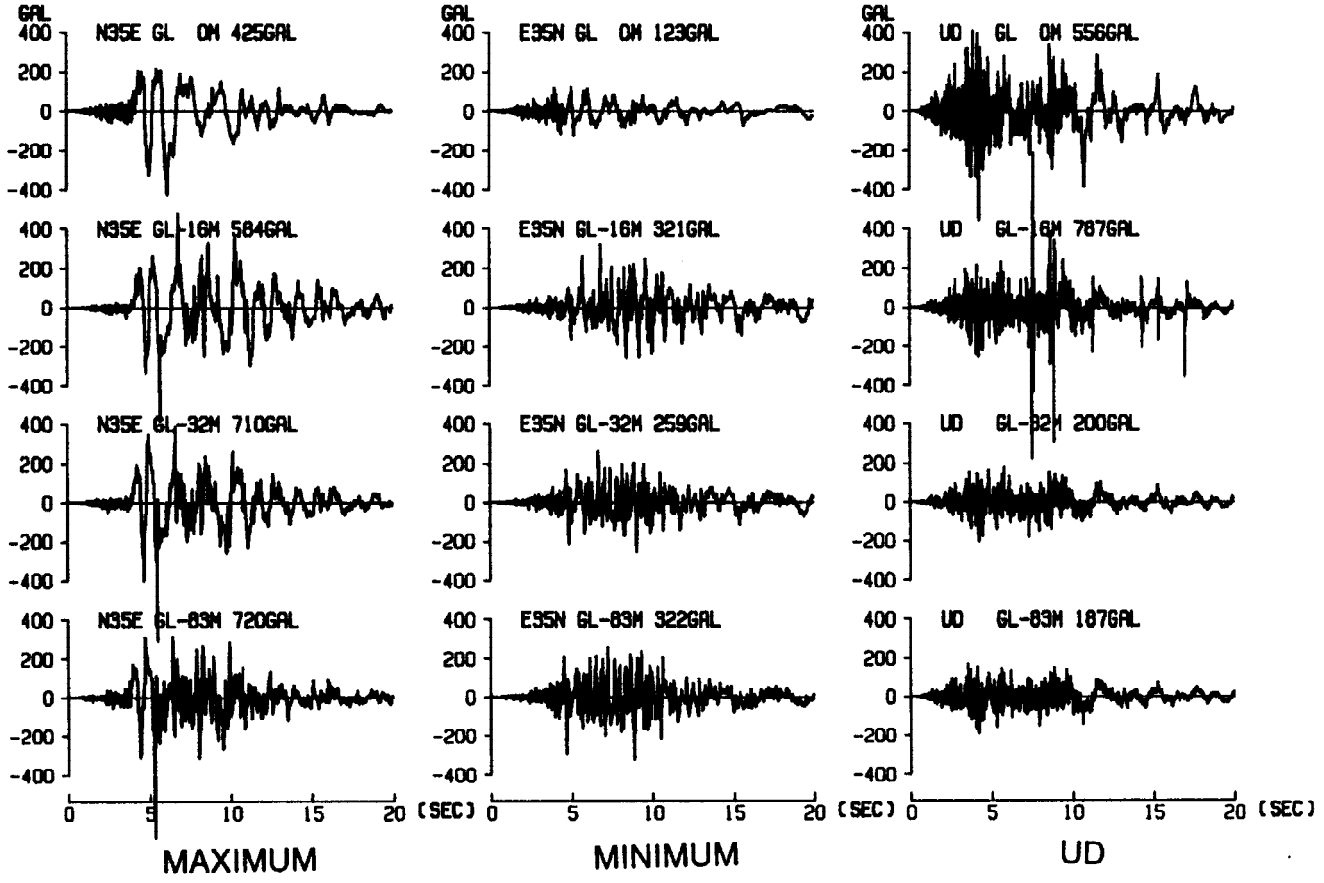

Fig.2 Observed accelerograms on the surface (GL0m) and in the boreholes (GL-16m, -32m, and -83m).

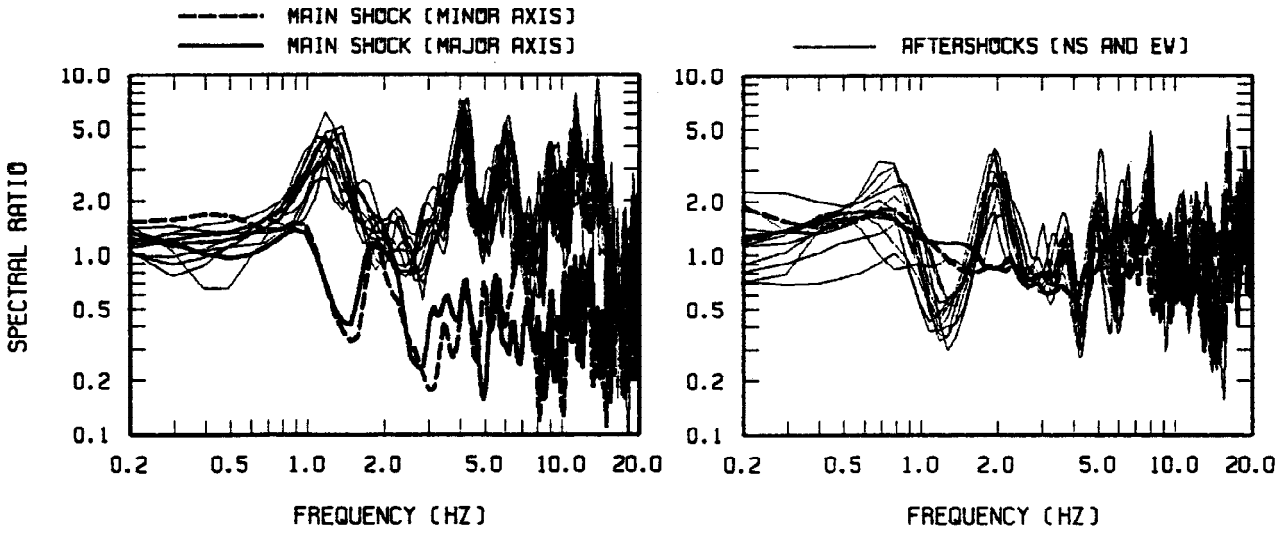

(a) GL0m/GL-32m (b) GL-32m/GL-83m

Fig.3 Fourier spectral ratios of station pairs for horizontal components of the main shock and aftershocks

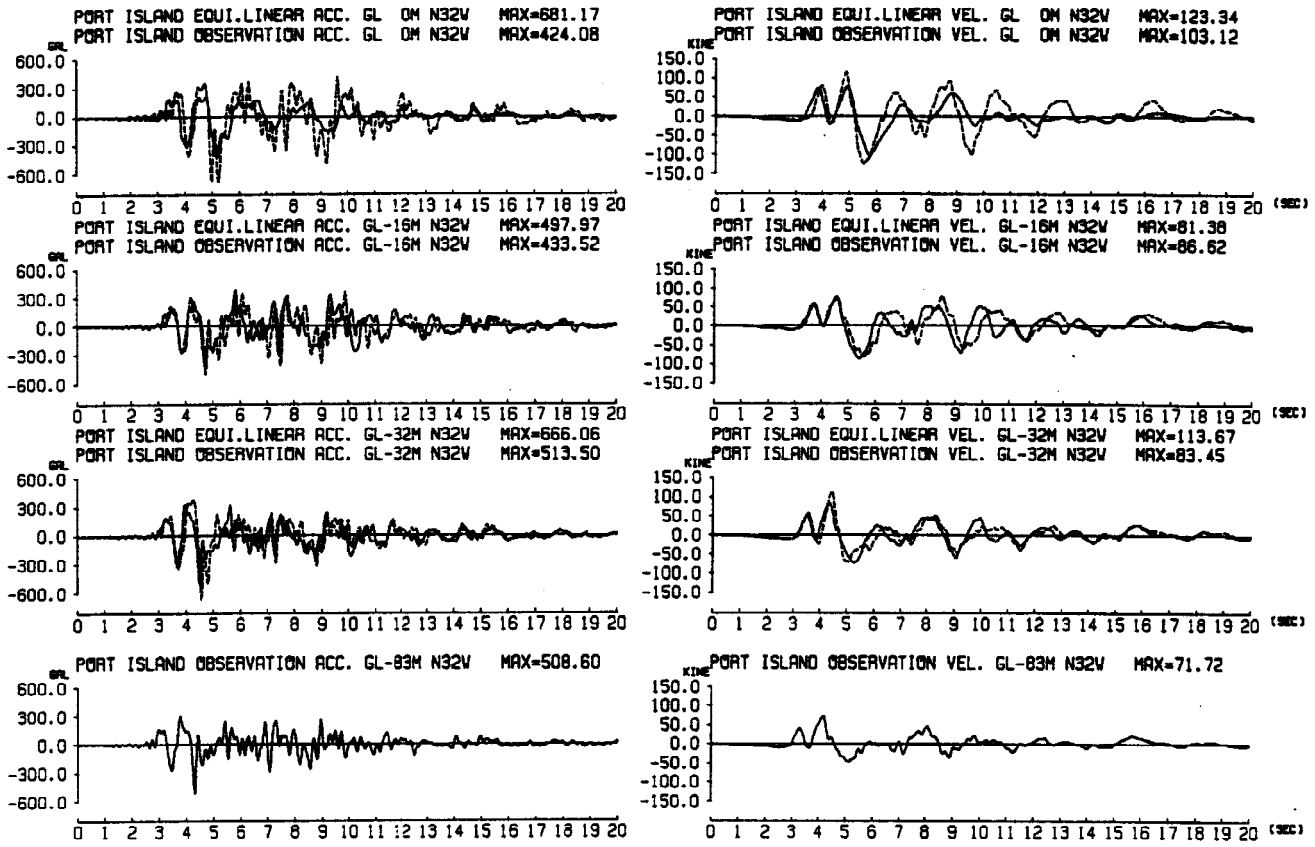

(a) Acceleration (b) Velocity

Fig.4 Comparison of time histories observed and simulated by the 1-D equivalent linear analysis. N32°W component is used as an input

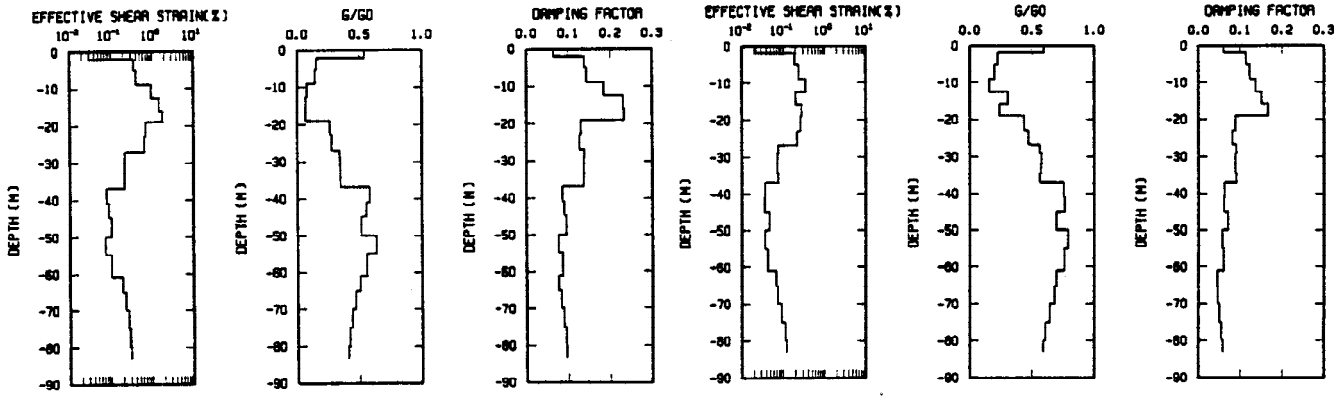

(a) N32°W component (b) E32°N component

Fig.5 Vertical distributions of the effective shear strain, shear modulus reduction factor, and the damping coefficient at 1 Hz obtained from the equivalent linear analysis.

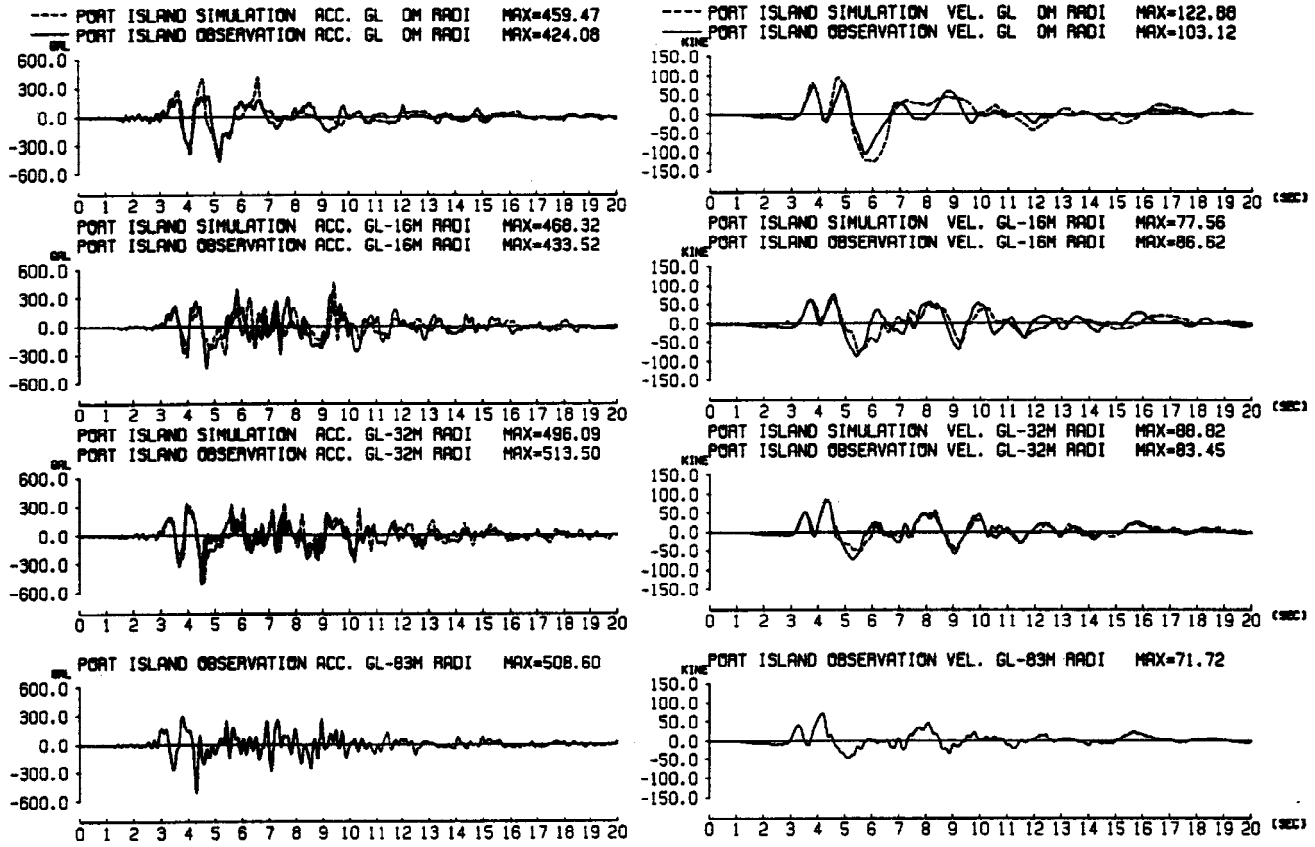

(a) Acceleration (b) Velocity

Fig.6 Comparison of time histories observed and simulated by the 1-D effective stress analysis. N32°W component is used as an input

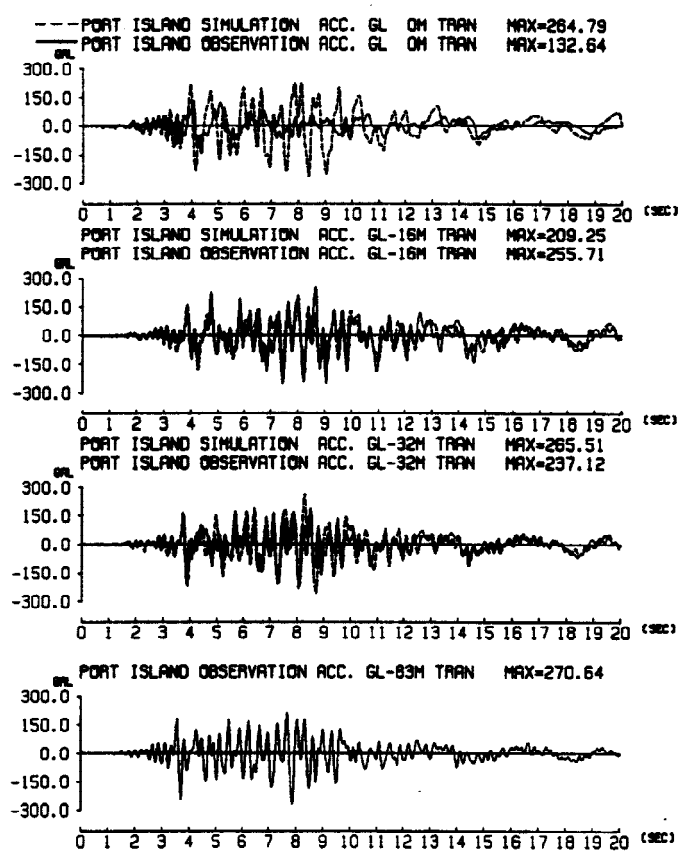

Fig.7 Comparison of accelerograms observed and simulated by the 1-D effective stress analysis. E32°N component is used as an input

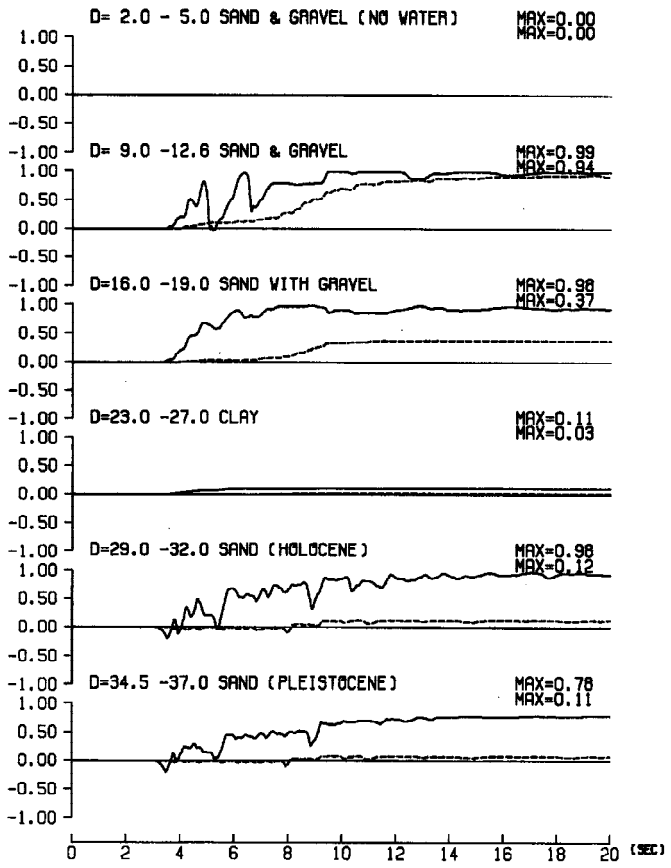

Fig.8 Time histories of the excess pore water pressure ratio calculated by the effective stress analysis. N32°W component (solid lines) or E32°N component (dotted lines) is used as an input.

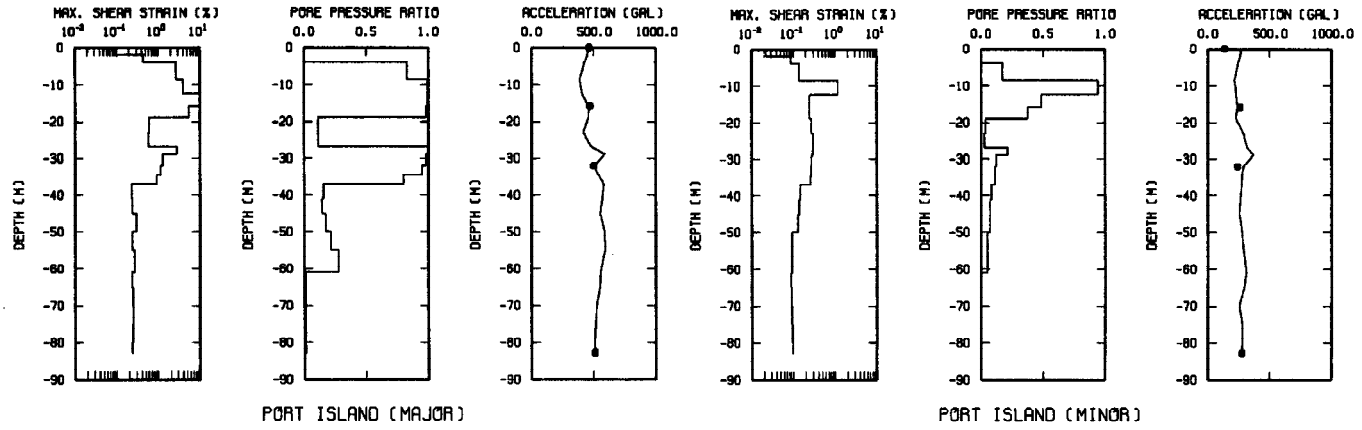

(a) N32°W component

(b) E32°N component

Fig.9 Vertical distributions of the maximum shear strain, the excess pore water pressure ratio, and the peak ground acceleration (PGA) obtained from the effective stress analysis.